

Single ion spectroscopy of four metastable state clear-out transitions in Yb II: isotope shifts and hyperfine structure

N. A. Diepeveen,¹ C. Robalo Pereira,¹ M. Mazzanti,¹ Z. E. D. Ackerman,¹
L. P. H. Gallagher,¹ T. Timmerman,¹ R. Gerritsma,^{1,2} and R. X. Schüssler¹

¹*Van der Waals-Zeeman Institute, Institute of Physics, University of Amsterdam, 1098 XH Amsterdam, Netherlands*

²*QuSoft, Science Park 123, 1098 XG Amsterdam, the Netherlands*

(Dated: August 15, 2024)

We present spectroscopic data for four metastable state clear-out transitions between 399 nm and 412 nm for all even long-lived isotopes of Yb⁺ as well as their hyperfine structure in ¹⁷¹Yb⁺. The strong ²D_{3/2} → ¹[1/2]_{1/2} transition at 412 nm represents an attractive alternative for the standard 935 nm repumper used in cooling and trapping experiments, while the transition to the ³[3/2]_{3/2} state at 411 nm clears out the ²F_{7/2} state, for which typically 638 nm or 760 nm are used. These two alternative transitions simplify the experimental setup by removing the need for infrared optics to cool and manipulate Yb⁺ and may be of particular interest when considering integrated photonics solutions. We also present data for the transitions ²D_{3/2} → ³[1/2]_{3/2} at 399 nm, and ²D_{3/2} → ¹[5/2]_{5/2} at 410 nm including decay branching ratios of the excited states.

I. INTRODUCTION

The spectrum of Yb⁺ has been studied extensively [1–4], motivated by its application in astronomy [5–8], as well as its broad use in quantum technologies [9, 10]. Moreover, precise spectroscopic data is used to benchmark and improve atomic structure calculations [11–18]. Rapid developments in trapping and laser cooling of single ions have greatly enhanced the precision of ion spectroscopy. In particular, using single laser cooled ions eliminates uncertainties due to Doppler broadening, background gas collisions and interactions between the ions. This has propelled the development of atomic clocks [19–21] and allowed tests of fundamental physics [22–25]. Yb⁺ possesses a complex level structure owing to large configuration interactions and spin-orbit couplings. Theoretical predictions for the strongest optical transitions in Yb⁺ have been published by Fawcett et al. [11] and Biémont et al. [12]. So far, most spectroscopic works on single Yb⁺ ions have focused on the narrow, dipole-forbidden transitions [26–29] and the dipole transitions used in laser cooling [30–34]. Many of the vast number of optical transitions have not been explored for their potential applications in laser cooling, trapping, and manipulation of the ions.

In this paper, we report spectroscopic data for four clear-out transitions that can be used to pump Yb⁺ out of the metastable ²D_{3/2} or ²F_{7/2} states. We determine the transition frequencies for all stable even isotopes as well as the hyperfine splittings of ¹⁷¹Yb⁺.

A summary of our results is given in Fig. 1 and Tab. I and Tab. II. Furthermore, we investigate the usefulness of the studied transitions in laser cooling and state manipulation of trapped ions. We find that the ²D_{3/2} → ¹[1/2]_{1/2} transition at 412 nm is very strong with a minimum linewidth of ~ 23(8) MHz at vanishing laser power and the transition is easily broadened to hundreds of MHz with modest laser power (see Sec. III A). This transition offers a potential alternative to the 935 nm transition that is more commonly used as a

repumper [30].

Additionally, we study the 411 nm clear-out transition of the extremely long-lived ²F_{7/2} state to the ³[3/2]_{3/2} state (see Sec. III D). Although we only have limited power available (< 3 mW) to drive this quadrupole transition, we find that the clear-out process is competitive with the more commonly used 760 nm and 638 nm solutions [26]. Finally, we study the ²D_{3/2} → ³[1/2]_{3/2} transition at 399 nm (see Sec. III B) as well as the ²D_{3/2} → ¹[5/2]_{5/2} transition at 410 nm (see Sec. III C) including the decay paths from the upper states. These results may be used to benchmark atomic structure calculations.

II. EXPERIMENTAL SETUP

We trap a single Yb⁺ ion in linear Paul trap. The trap is driven by a radio frequency field of 5.8 MHz, resulting in secular trap frequencies of $\omega_{x,y,z} = 2\pi \times (400, 400, 120)$ kHz (see [37] for more details). Excess micromotion was compensated to amplitudes $\lesssim 50$ nm.

A level scheme of the relevant transitions for this work in ¹⁷¹Yb⁺ is shown in Fig. 1. The Yb⁺ ions are produced by first heating up a sample of atomic Yb which is then ionized by a two-photon process in the trap center. For the first ionization step a 398.9 nm laser is used and excites the ¹S₀ → ¹P₁ transition of the target isotope. A laser at 369 nm is used for the second step of the ionisation process as well as for Doppler cooling on the ²S_{1/2} → ²P_{1/2} transition in Yb⁺. There is a weak decay path of 0.5 % from the ²P_{1/2} state to the metastable ²D_{3/2} state which has a lifetime of ~52 ms [38, 39]. Therefore, we use a 935 nm laser to pump the population back to the cooling cycle via excitation to the ³[3/2]_{1/2} state. Furthermore, the ion can also populate the long-lived ²F_{7/2} state. We use a laser at 760 nm to excite the population to the ¹[3/2]_{3/2} state from which it can decay back to the cooling cycle.

In order to cool and image ¹⁷¹Yb⁺, the hyperfine split-

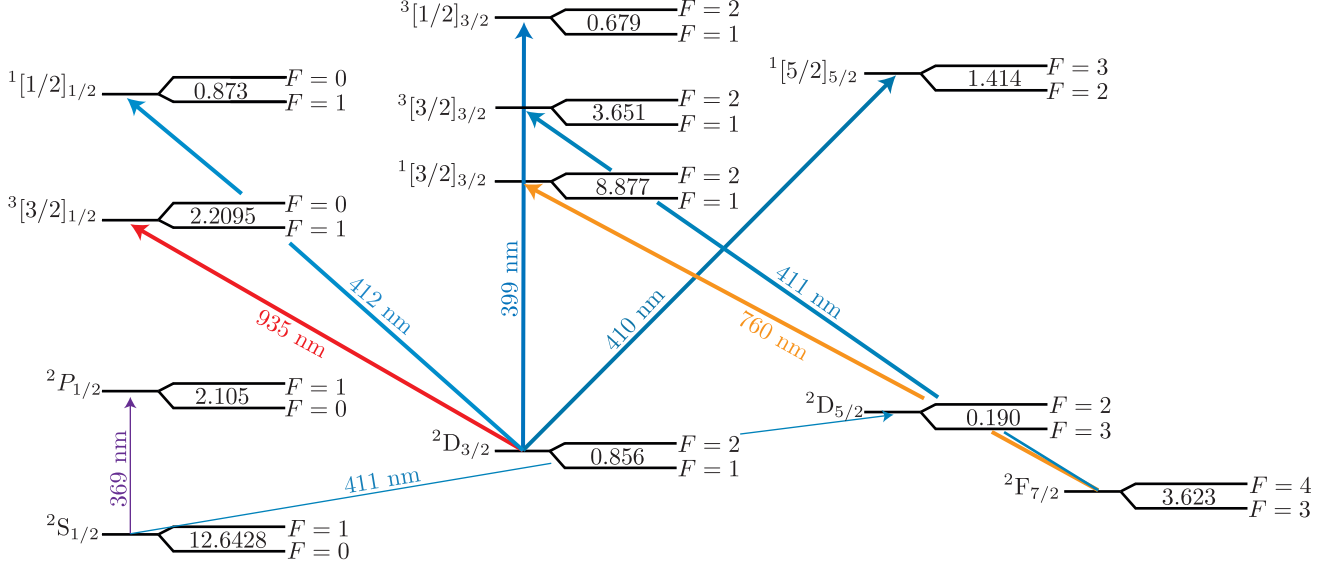


FIG. 1. Level scheme for $^{171}\text{Yb}^+$: the transitions indicated in bold are measured in this work. The measured hyperfine splittings of these transitions are given in GHz with an uncertainty of 10 MHz. The hyperfine splitting of the other states are also in GHz and are taken from: $^2\text{P}_{1/2}$ [9], $^2\text{D}_{5/2}$ [35], $^2\text{S}_{1/2}$ [36]. The hyperfine splittings of the $^2\text{D}_{3/2}$ and $^2\text{F}_{7/2}$ states are the average of all measured lines.

| Lower state | $^2\text{D}_{3/2}$ | | $^2\text{F}_{7/2}$ | | | |
|-------------|--------------------|-----------------|--------------------|-----------------|-----------------|-----------------|
| Upper state | $^1[1/2]_{1/2}$ | $^3[1/2]_{3/2}$ | $^1[5/2]_{5/2}$ | $^3[3/2]_{1/2}$ | $^3[3/2]_{3/2}$ | $^1[3/2]_{3/2}$ |
| Isotope | 412 nm | 399 nm | 410 nm | 935 nm | 411 nm | 760 nm |
| 168 | 727 533 757 | 751 394 594 | 730 548 033 | 320 562 140 | 729 061 398 | 394 432 870 |
| 170 | 727 537 172 | 751 395 899 | 730 550 738 | 320 565 870 | 729 056 942 | 394 429 590 |
| 172 | 727 540 360 | 751 397 112 | 730 553 260 | 320 569 350 | 729 052 770 | 394 426 550 |
| 174 | 727 542 754 | 751 397 858 | 730 555 133 | 320 571 970 | 729 049 536 | 394 424 150 |
| 176 | 727 545 028 | 751 398 779 | 730 556 908 | 320 574 460 | 729 046 459 | 394 421 890 |

TABLE I. Frequencies of the four investigated transitions for even isotopes. For completeness we have included the measurement results for the clear-out transitions at 935 nm and 760 nm. All frequencies are given in MHz. The uncertainties are quoted to be 30 MHz (for more details see text). For the four blue transitions the statistical uncertainties of the measurements are below 1 MHz. For the 935 nm and 760 nm transitions, the frequencies were determined by a rough frequency scan documented only at the 10 MHz level.

| 412 nm | | 399 nm | | 410 nm | |
|---|-------------|---|-------------|---|-------------|
| $ ^2\text{D}_{3/2}, F\rangle \rightarrow ^1[1/2]_{1/2}, F'\rangle$ | | $ ^2\text{D}_{3/2}, F\rangle \rightarrow ^3[1/2]_{3/2}, F'\rangle$ | | $ ^2\text{D}_{3/2}, F\rangle \rightarrow ^1[5/2]_{5/2}, F'\rangle$ | |
| $F = 2 \rightarrow F' = 1$ | 727 537 711 | $F = 2 \rightarrow F' = 1$ | 751 395 524 | $F = 2 \rightarrow F' = 2$ | 730 550 429 |
| $F = 1 \rightarrow F' = 1$ | 727 538 567 | $F = 2 \rightarrow F' = 2$ | 751 396 206 | $F = 1 \rightarrow F' = 2$ | 730 551 286 |
| $F = 1 \rightarrow F' = 0$ | 727 539 440 | $F = 1 \rightarrow F' = 1$ | 751 396 380 | $F = 2 \rightarrow F' = 3$ | 730 551 845 |
| – | – | $F = 1 \rightarrow F' = 2$ | 751 397 059 | – | – |

| 935 nm | | 760 nm | | 411 nm | |
|---|-------------|---|-------------|---|-------------|
| $ ^2\text{D}_{3/2}, F\rangle \rightarrow ^3[3/2]_{1/2}, F'\rangle$ | | $ ^2\text{F}_{7/2}, F\rangle \rightarrow ^1[3/2]_{3/2}, F'\rangle$ | | $ ^2\text{F}_{7/2}, F\rangle \rightarrow ^3[3/2]_{3/2}, F'\rangle$ | |
| $F = 2 \rightarrow F' = 1$ | 320 566 177 | $F = 3 \rightarrow F' = 1$ | 394 424 969 | $F = 3 \rightarrow F' = 1$ | 729 055 214 |
| $F = 1 \rightarrow F' = 1$ | 320 567 035 | $F = 4 \rightarrow F' = 2$ | 394 430 225 | $F = 4 \rightarrow F' = 2$ | 729 055 244 |
| $F = 1 \rightarrow F' = 0$ | 320 569 244 | $F = 3 \rightarrow F' = 2$ | 394 433 848 | $F = 3 \rightarrow F' = 2$ | 729 058 866 |

TABLE II. Frequencies of the hyperfine transitions in $^{171}\text{Yb}^+$ for the investigated transitions. For completeness we have included the measurement results for the clear-out transitions at 935 nm and 760 nm. All frequencies given in MHz. Uncertainties are quoted to be 30 MHz, while statistical uncertainties from a Lorentzian fit to the data are all below 1 MHz.

tings of the transitions need to be bridged. We use a 14.7 GHz electro-optic modulator (EOM) for the 369 nm Doppler transition, a 3.07 GHz fiber EOM for the 935 nm repumper, and a 5.26 GHz fiber EOM for the 760 nm clear-out transition. Microwaves at 12.6 GHz to bridge the ground state hyperfine splitting can also be supplied using a microwave horn [9].

We image the ion's fluorescence at 369 nm wavelength on an EMCCD camera. The 935 nm and 760 nm lasers are aligned along the axial axis of the linear trap. A magnetic field of ~ 0.3 mT, oriented perpendicular to the trap axis, is used to avoid coherent population trapping during Doppler cooling. The 369 nm laser and the blue spectroscopy lasers enter at an angle of 45° to the axial direction and 90° to the magnetic field. We avoid the use of circular laser polarization to minimize optical pumping effects that may cause line shifts.

Two lasers are used to measure the four transitions. The frequency of the three studied transitions spanning the 410-412 nm range are easily reached by tuning the wavelength of the 411 nm laser that is normally used for driving the $^2S_{1/2} \rightarrow ^2D_{5/2}$ clock transition [40]. The 399 nm transition from $^2D_{3/2} \rightarrow ^3[1/2]_{3/2}$ is reached with a home-built laser based on [41]. It is noteworthy that this transition is only ~ 130 GHz away from the first step ionization laser that drives the $^1S_0 \rightarrow ^1P_1$ transition in neutral Yb.

III. RESULTS

All lasers are locked to a wavemeter (High Finesse WS8-10) using a computer controlled feedback loop. The wavemeter is calibrated with a 638 nm laser from a neighbouring laboratory locked to the $^1S_0 \rightarrow ^3P_1$ clock transition in ^{88}Sr at 434.829 121 300(20) THz [42, 43]. This laser has a linewidth of 1.2 kHz and drifts about 10 kHz per day. The wavemeter calibration is quoted to be valid for 1 h with an error of 10 MHz for wavelengths within a ± 200 nm range around the calibration wavelength. Outside of this range, where the presented results fall, the measured values are shifted and the uncertainty is stated to be 30 MHz [44]. To estimate this systematic shift, we measured the $^2S_{1/2} \rightarrow ^2D_{5/2}$ clock transition for $^{174}\text{Yb}^+$ several times over the span of two weeks to be 729 475 284(2)_{stat} MHz which differs by only ~ 0.2 MHz from the best known value [25]. Therefore, we expect our results to be more precise than the quoted uncertainty of the 30 MHz. We quote an uncertainty of 10 MHz for the hyperfine splittings, but a more conservative 30 MHz uncertainty for the frequencies of the optical transitions.

The frequencies of the transitions were determined by scanning the lasers on a MHz level while simultaneously collecting the fluorescence of a single trapped ion on the camera for a set detection time. For each single fluorescence measurement the frequency of the laser was read out using the wavemeter, i.e. our data consists of unique laser frequencies paired with a number of detected photons.

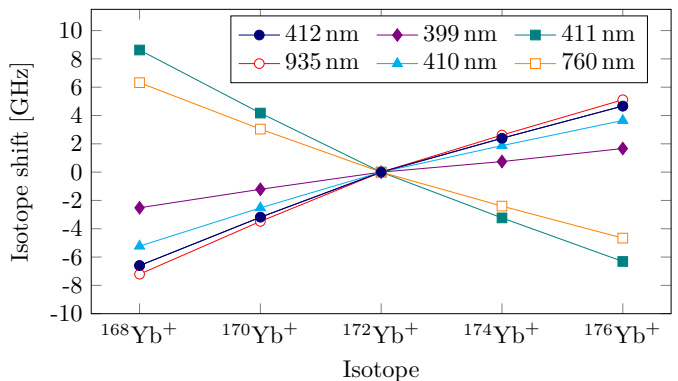


FIG. 2. The isotope shifts for the six measured transitions with the result for $^{172}\text{Yb}^+$ taken as the reference. The uncertainty of 30 MHz is smaller than the marker size.

For all data with the exception of the 412 nm and 935 nm transitions, a pulsed scheme was used to measure the frequencies. Here, the fluorescence data was analysed by projecting it on one of two outcomes. A threshold was set on the measured photon counts to distinguish the cases where the ion was in the bright ($^2S_{1/2}$, $^2D_{3/2}$) state and the dark ($^2F_{7/2}$) state. Owing to the long lifetime of the dark state, the detection error can be made negligible by increasing the detection time [45]. From the Lorentzian fit to the data we get typical statistical uncertainties of ~ 200 kHz for the frequencies with outliers of 700 kHz for the low-abundant $^{168}\text{Yb}^+$. These are negligible compared to the wavemeter uncertainty and we quote the latter as the dominant error. The hyperfine splittings in $^{171}\text{Yb}^+$ were extracted from a combined fit to all transitions.

A. $^2D_{3/2} \rightarrow ^1[1/2]_{1/2}$ at 412 nm

We used the 369 nm laser and scanned the spectroscopy laser around the predicted value of 412 nm [11, 12]. On resonance, the 412 nm acts as a repumper for the $^2D_{3/2}$ state, resulting in a peak in ion fluorescence. We recorded the ion fluorescence for 100 ms for each measurement. Such a dataset is shown in Fig. 3 for the hyperfine transitions, with the data averaged in 4 MHz bins for clarity. For $^{171}\text{Yb}^+$, we observe three peaks in the fluorescence spectrum, corresponding to the three dipole-allowed hyperfine transitions. To enhance the signal intensity for the $|^2D_{3/2}, F = 2\rangle \rightarrow |^1[1/2]_{1/2}, F = 1\rangle$ transition, we tuned the 935 nm laser on the $|^2D_{3/2}, F = 1\rangle \rightarrow |^3[3/2]_{1/2}, F = 1\rangle$ transition to assist in pumping the population to the $|^2D_{3/2}, F = 2\rangle$ state. The two lowest frequencies have a difference of 858(10) MHz, in agreement with the known hyperfine splitting of the $^2D_{3/2}$ state [9] and we identify them as the $|^2D_{3/2}, F = 2\rangle \rightarrow |^1[1/2]_{1/2}, F = 1\rangle$ and $|^2D_{3/2}, F = 1\rangle \rightarrow |^1[1/2]_{1/2}, F = 1\rangle$ transitions. The third peak is 873(10) MHz higher and we attribute it to the $|^2D_{3/2}, F = 1\rangle \rightarrow |^1[1/2]_{1/2}, F = 0\rangle$ transition. It is noted that the hyperfine structure of the

$^1[1/2]_{1/2}$ state is inverted.

For completeness and comparison, we performed the same measurement procedure on the $^3D_{3/2} \rightarrow ^3[3/2]_{1/2}$ transition using the 935 nm laser instead of the 412 nm laser. We used For $^{171}\text{Yb}^+$, we again find three fluorescence peaks as shown in Fig. 3. The difference between the three peaks is 858(10) MHz and 2209(10) MHz, which is in agreement with literature values [9] for the hyperfine splittings of the two states.

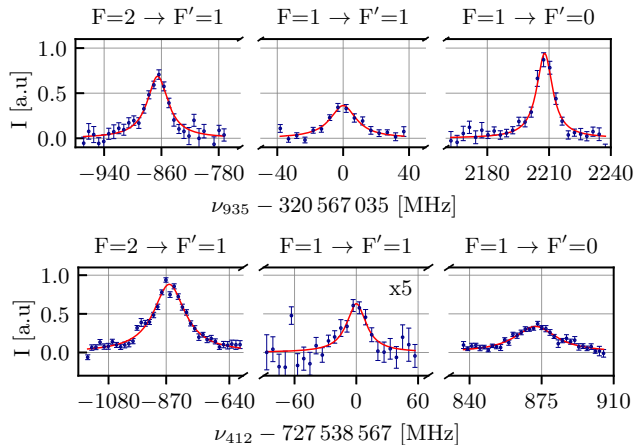


FIG. 3. Ion fluorescence (I) as a function of frequency for the hyperfine structure of the levels involved in the $^2D_{3/2} \rightarrow ^3[3/2]_{1/2}$ transition at 935 nm (top) and the $^2D_{3/2} \rightarrow ^1[1/2]_{1/2}$ transition at 412 nm (bottom). In each set, the peaks are normalised to the largest peak and the data points represent an average of 4 MHz bins. The amplitude of the transition from $F = 1 \rightarrow F' = 1$ in the bottom graph is scaled by a factor of 5 to enhance its visibility relative to the other peaks. The red line indicates a Lorentzian fit, for more details see Sec. III A.

For the 412 nm transition, laser powers as low as $1 \mu\text{W}$ with an estimated beam waist of $390(40) \mu\text{m}$ were enough to achieve repumping rates that are competitive with the 935 nm beam at $200 \mu\text{W}$ with a beam waist of $360(30) \mu\text{m}$ for the even isotopes. We measured the transition linewidth of the 412 transition for different laser powers in $^{174}\text{Yb}^+$, as depicted in Fig. 4. Extrapolating to zero laser power, we estimate an upper limit of the natural linewidth of $23(8)$ MHz. Remarkably, at only a few mW of power, the linewidth is broadened to several hundreds of MHz. In our setup, ~ 11 mW should be enough to have a linewidth similar to the hyperfine splitting of the $^2D_{3/2}$ state in $^{171}\text{Yb}^+$, eliminating the need for an EOM.

B. $^2D_{3/2} \rightarrow ^3[1/2]_{3/2}$ at 399 nm

The ion was prepared in the $^2D_{3/2}$ state using a $100 \mu\text{s}$ pulse of 369 nm light. A 2 ms spectroscopy pulse at 399 nm then excited the ion to the $^3[1/2]_{3/2}$ state, followed by a 20 ms fluorescence measurement using the 369 nm and 935 nm lasers. The $^3[1/2]_{3/2}$ state has a

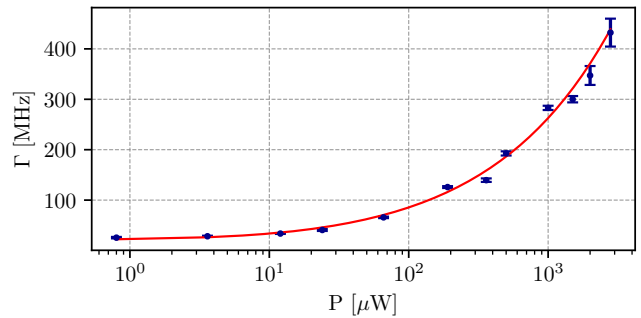


FIG. 4. Linewidth as a function of laser power for the $^2D_{3/2} \rightarrow ^1[1/2]_{1/2}$ transition at 412 nm. The data is fitted with a Lorentzian function and gives an extrapolated linewidth, for vanishing laser power, of $\Gamma = 23(8)$ MHz. For these measurements, the 369 nm Doppler laser's power was set to saturate the cooling transition.

dipole-allowed decay channel to the $^2D_{5/2}$ state from which it can subsequently decay to the long-lived $^2F_{7/2}$ state, that remains dark during fluorescence detection. We identified the resonance of the 399 nm transition with a reduction in ion fluorescence. After fluorescence detection, the 760 nm laser cleared out the $^2F_{7/2}$ state before the start of the next measurement.

In order to determine the branching ratio, we added a wait time of 50 ms after the 399 nm pulse, to let the $^2D_{5/2}$ state decay. We assume there is no significant direct decay on the $^3[1/2]_{3/2} \rightarrow ^2F_{7/2}$ quadrupole transition. Considering the branching ratio of 17% of $^2D_{5/2}$ to $^2S_{1/2}$ state [26], we find the branching ratio between the decay paths $^3[1/2]_{3/2} \rightarrow ^2S_{1/2}$ and $^3[1/2]_{3/2} \rightarrow ^2D_{5/2}$ to be $8.4(1.4)$.

For measuring the hyperfine structure in $^{171}\text{Yb}^+$, we increased the spectroscopy pulse of 399 nm to 50 ms and kept the 369 nm and 935 nm lasers on. The latter was tuned to clear out the hyperfine level that is not targeted by the 399 nm laser. We observe four distinct dips, as shown in Fig. 5. We find two sets of frequencies that are $854(10)$ MHz apart, corresponding to $^2D_{3/2}$ hyperfine splitting. The frequency difference of the other two sets of $679(10)$ MHz gives the splitting of the $^3[1/2]_{3/2}$ state.

The ordering of the hyperfine levels of $^3[1/2]_{3/2}$ was found by determining the hyperfine level of the $^2F_{7/2}$ state that the ion decayed to. From the $|^3[1/2]_{3/2}, F = 1\rangle$ state, it can only decay to $|^2D_{5/2}, F = 2\rangle$ due to selection rules. When it does not decay to the $^2S_{1/2}$ ground state, the $|^2D_{5/2}, F = 2\rangle$ state can only decay to the $|^2F_{7/2}, F = 3\rangle$ state while the $|^2D_{5/2}, F = 3\rangle$ state predominantly decays to $|^2F_{7/2}, F = 4\rangle$. We determined the final hyperfine level of the $^2F_{7/2}$ state that the ion decayed to using the 760 nm transition, for which all the hyperfine splitting and levels are known. The assignment of the transitions is shown in Fig. 5. We note that the hyperfine structure of the $^3[1/2]_{3/2}$ state is not inverted.

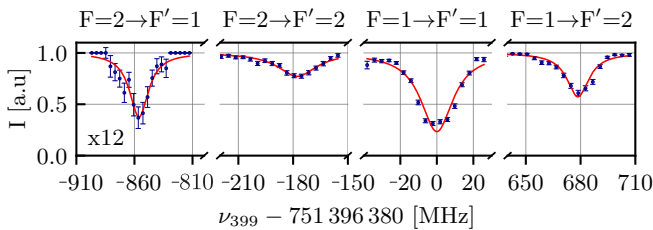


FIG. 5. Ion fluorescence (I) as a function of frequency for the hyperfine structure of the levels involved in the ${}^2D_{3/2} \rightarrow {}^3[1/2]_{3/2}$ transition at 399 nm. The data points represent an average of 4 MHz bins. The amplitude of the transition from $F = 2 \rightarrow F' = 1$ is scaled by a factor of 12 to enhance its visibility relative to the other dips. The red line indicates a Lorentzian fit, for more details see Sec. III B.

C. ${}^2D_{3/2} \rightarrow {}^1[5/2]_{5/2}$ at 410 nm

We used a pulsed scheme similar to Sec. III B, where we pumped the ion to the ${}^2D_{3/2}$ state for 100 μs and then performed a 5 ms spectroscopy pulse of 410 nm light to excite the ion to the ${}^1[5/2]_{5/2}$ state. This state can decay to the ${}^2D_{5/2}$ state and subsequently to the ${}^2F_{7/2}$ state. As before, we measured a reduction in fluorescence when the 410 nm laser was on resonance.

For ${}^{171}\text{Yb}^+$, we find three dips of fluorescence. Since the smallest frequencies are separated by 856(10) MHz, we can identify them as the $|{}^2D_{3/2}, F = 1\rangle \rightarrow |{}^1[5/2]_{5/2}, F = 2\rangle$ and $|{}^2D_{3/2}, F = 2\rangle \rightarrow |{}^1[5/2]_{5/2}, F = 2\rangle$ transitions. The third frequency corresponds to $|{}^2D_{3/2}, F = 2\rangle \rightarrow |{}^1[5/2]_{5/2}, F = 3\rangle$, giving a hyperfine splitting of 1414(10) MHz for the ${}^1[5/2]_{5/2}$ state. The data is shown in Fig. 6. The hyperfine structure of the ${}^1[5/2]_{5/2}$ state is not inverted.

To check that there is no direct decay on the ${}^1[5/2]_{5/2} \rightarrow {}^2F_{7/2}$ quadrupole transition, we perform a branching ratio measurement with ${}^{174}\text{Yb}^+$. For this we used a 2 ms pulse to pump the ion in the ${}^2D_{3/2}$ state, followed by a 10 ms pulse of 410 nm light. We detected the fluorescence after waiting 50 ms, allowing all population in the ${}^2D_{5/2}$ state to decay. We observed the ion in the ground state in 18(1)% of the cases, for all pumping times $>300 \mu\text{s}$ and independent of the pulse length of 410 nm light. This result is in agreement with the known branching ratio of the ${}^2D_{5/2}$ state [26]. We therefore do not find measurable decay on the ${}^1[5/2]_{5/2} \rightarrow {}^2F_{7/2}$ quadrupole transition.

D. ${}^2F_{7/2} \rightarrow {}^3[3/2]_{3/2}$ at 411 nm

To measure the transition frequency, we prepared the ion in the ${}^2F_{7/2}$ state using a 30 ms pulse of 369 nm and 399 nm light, see Sec. III B. A pulse of 411 nm light then excited the ion to the ${}^3[3/2]_{3/2}$ state, from where it could decay back to the bright states, resulting in a fluorescence peak when the 411 nm laser is resonant.

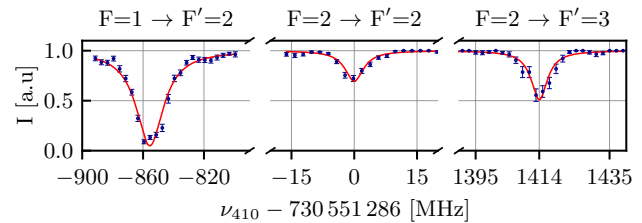


FIG. 6. Ion fluorescence (I) as a function of frequency for the levels involved in the ${}^2D_{3/2} \rightarrow {}^1[5/2]_{5/2}$ transition at 410 nm. The data points represent an average of 4 MHz bins. The red line indicates a Lorentzian fit, for more details see Sec. III C.

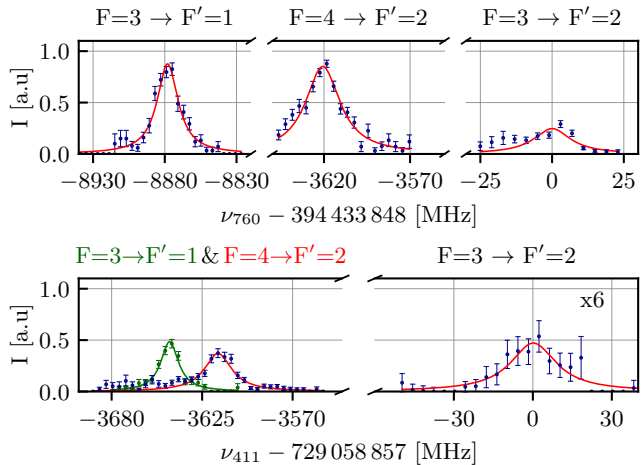


FIG. 7. Ion fluorescence (I) as a function of frequency for the hyperfine structure of the levels involved in the ${}^2F_{7/2} \rightarrow {}^3[3/2]_{3/2}$ transition at 760 nm (top) and ${}^2F_{7/2} \rightarrow {}^3[3/2]_{3/2}$ transition at 411 nm (bottom). The data points represent an average of 4 MHz bins. The amplitude of the transition from $F = 3 \rightarrow F' = 2$ in the bottom graphs is scaled by a factor of 6 to enhance its visibility relative to the other peaks. The red line indicates a Lorentzian fit, for more details see Sec. III D.

We measured the hyperfine structure of ${}^{171}\text{Yb}^+$ using the 399 nm laser, discussed in section Sec. III B, to pump the ion to the $|{}^2F_{7/2}, F = 3\rangle$ state. The frequency difference of 3651(10) MHz between the two observed transitions corresponds to the hyperfine splitting of the ${}^3[3/2]_{3/2}$ state. Additionally, by exciting the ion to the $|{}^2F_{7/2}, F = 4\rangle$ state and measuring the third transition, we were able to assign the hyperfine levels. We measure a difference of 3622(10) MHz to the higher of the other two frequencies, in agreement with the hyperfine splitting of the ${}^2F_{7/2}$ state [31]. We note that the hyperfine structure of the ${}^3[3/2]_{3/2}$ state is not inverted.

For completeness and in order to enable comparison, we measured the hyperfine splittings of the 760 nm transition. Here, the roles of the 760 nm and 411 nm lasers were reversed compared to the previous measurement. The three measured peaks, shown in Fig. 7, give the known hyperfine splitting of the ${}^2F_{7/2}$ state. The splitting of the upper state ${}^3[3/2]_{3/2}$ was measured to be 8877(10) MHz,

in agreement with previous values [46].

With the 411 nm laser we were limited to around ~ 2.3 mW laser power with a waist of $390(40)$ μm , leading to a slower clear-out process than for the 760 nm laser, for which we had 55 mW available with a waist of $360(30)$ μm . This is reflected in the maximum repump efficiency of 50% during a 100 ms pulse as shown in the hyperfine measurement, see Fig. 7. This could easily be improved by using more laser power.

IV. CONCLUSION

We have presented spectroscopic data for four clear-out transitions in Yb^+ . The strong $^2D_{3/2} \rightarrow ^1[1/2]_{1/2}$ transition at 412 nm forms an attractive alternative for the standard 935 nm repumper, while the transition at 410 nm clears out the $^2F_{7/2}$ state via the $^3[3/2]_{3/2}$ state. We note that it is quite remarkable that all transitions that are needed for photoionizing Yb, laser cooling and manipulation of the ions fall within the narrow wave-

length window of 369-412 nm. This property is not shared by the simpler heavy earth-alkaline ions Ca^+ , Sr^+ and Ba^+ that have metastable states and are often used in cooling and trapping experiments. This feature may be of practical use when considering integration of optical elements in micro fabricated ions traps which would be simpler to produce for a narrow range of wavelengths [47].

In the future, further narrowing of the wavelength window would be achieved by studying the $^2D_{3/2} \rightarrow ^3[1/2]_{1/2}$ clear-out transition at 378 nm, as well as the $^2F_{7/2} \rightarrow ^3[3/2]_{5/2}$ and $^2F_{7/2} \rightarrow ^3[1/2]_{3/2}$ clear-out transitions at 372 and 376 nm, respectively.

ACKNOWLEDGEMENTS

We thank the group of Florian Schreck for making available the Sr clock laser for wavelength calibration. This work was supported by the Dutch Research Council (Grant Nos. 680.91.120, VI.C.202.051 and 680.92.18.05, R.G., M.M. and R.X.S.).

-
- [1] R. W. Berends, E. H. Pinnington, B. Guo, and Q. Ji, Beam-laser lifetime measurements for four resonance levels of Yb II, *J. Phys. B: At. Mol. Opt. Phys.* **26**, L70 (1993).
- [2] E. H. Pinnington, R. W. Berends, and Q. Ji, Beam-laser lifetime measurements of Yb ii energy levels, *Phys. Rev. A* **50**, 2758 (1994).
- [3] E. H. Pinnington, G. Rieger, and J. A. Kernahan, Beam-laser measurements of the lifetimes of the $6p$ levels in Yb II, *Phys. Rev. A* **56**, 2421 (1997).
- [4] Z. S. Li, S. Svanberg, X. T. P. Quinet, and E. Biémont, Lifetime measurements in Yb II with time-resolved laser spectroscopy, *Journal of Physics B: Atomic, Molecular and Optical Physics* **32**, 1731 (1999).
- [5] S. Honda, W. Aoki, T. Kajino, H. Ando, T. C. Beers, H. Izumiura, K. Sadakane, and M. Takada-Hidai, Spectroscopic studies of extremely metal-poor stars with the Subaru high dispersion spectrograph. ii. the r-process elements, including thorium*, *The Astrophysical Journal* **607**, 474 (2004).
- [6] François, P., Depagne, E., Hill, V., Spite, M., Spite, F., Plez, B., Beers, T. C., Andersen, J., James, G., Barbey, B., Cayrel, R., Bonifacio, P., Molaro, P., Nordström, B., and Primas, F., First stars* - viii. enrichment of the neutron-capture elements in the early galaxy, *A&A* **476**, 935 (2007).
- [7] Montelius, M., Forsberg, R., Ryde, N., Jönsson, H., Afşar, M., Johansen, A., Kaplan, K. F., Kim, H., Mace, G., Sneden, C., and Thorsbro, B., Chemical evolution of ytterbium in the galactic disk, *A&A* **665**, A135 (2022).
- [8] C. Sneden, J. E. Lawler, J. J. Cowan, I. I. Ivans, and E. A. D. Hartog, New rare earth element abundance distributions for the sun and five r-process-rich very metal-poor stars, *The Astrophysical Journal Supplement Series* **182**, 80 (2009).
- [9] S. Olmschenk, K. C. Younge, D. L. Moehring, D. N. Matsukevich, P. Maunz, and C. Monroe, Manipulation and detection of a trapped Yb^+ hyperfine qubit, *Phys. Rev. A* **76**, 052314 (2007).
- [10] C. Monroe, W. C. Campbell, L.-M. Duan, Z.-X. Gong, A. V. Gorshkov, P. W. Hess, R. Islam, K. Kim, N. M. Linke, G. Pagano, P. Richerme, C. Senko, and N. Y. Yao, Programmable quantum simulations of spin systems with trapped ions, *Rev. Mod. Phys.* **93**, 025001 (2021).
- [11] B. Fawcett and M. Wilson, Computed oscillator strengths, Landé g values, and lifetimes in Yb II, *Atomic Data and Nuclear Data Tables* **47**, 241 (1991).
- [12] E. Biémont, J.-F. Dutrieux, I. Martin, and P. Quinet, Lifetime calculations in Yb II, *Journal of Physics B: Atomic, Molecular and Optical Physics* **31**, 3321 (1998).
- [13] S. N. Lea, S. A. Webster, and G. P. Barwood, Polarizabilities and blackbody shifts in Sr^+ and Yb^+ , in *Proceedings of the 20th European Frequency and Time Forum* (2006) pp. 302-307.
- [14] U. I. Safronova and M. S. Safronova, Third-order relativistic many-body calculations of energies, transition rates, hyperfine constants, and blackbody radiation shift in $^{171}\text{Yb}^+$, *Phys. Rev. A* **123**, 022512 (2009).
- [15] V. A. Dzuba and V. V. Flambaum, Calculation of nuclear-spin-dependent parity nonconservation in s - d transitions of Ba^+ , Yb^+ , and Ra^+ ions, *Phys. Rev. A* **83**, 052513 (2011).
- [16] S. G. Porsev, M. S. Safronova, and M. G. Kozlov, Correlation effects in Yb^+ and implications for parity violation, *Phys. Rev. A* **86**, 022504 (2012).
- [17] J. Migdalek and W. Siegel, Relativistic E1 transition probabilities and lifetimes along Yb^+ isoelectronic sequence, *Journal of Physics B: Atomic, Molecular and Optical Physics* **45**, 145002 (2012).
- [18] A. Roy, S. De, B. Arora, and B. K. Sahoo, Polarizability and magic wavelength of Yb^+ clock transition $^2s_{1/2} \rightarrow ^2d_{3/2}$, in *2017 Joint Conference of the European Frequency and Time Forum and IEEE International Frequency Control Symposium (EFTF/IFCS)* (2017) pp.

- 753–757.
- [19] A. D. Ludlow, M. M. Boyd, J. Ye, E. Peik, and P. Schmidt, Optical atomic clocks, *Rev. Mod. Phys.* **87**, 637 (2015).
- [20] N. Huntemann, C. Sanner, B. Lipphardt, C. Tamm, and E. Peik, Single-ion atomic clock with 3×10^{-18} systematic uncertainty, *Phys. Rev. Lett.* **116**, 063001 (2016).
- [21] H. N. Hausser, J. Keller, T. Nordmann, N. M. Bhatt, J. Kiethe, H. Liu, M. von Boehn, J. Rahm, S. Weyers, E. Benkler, B. Lipphardt, S. Doerscher, K. Stahl, J. Klose, C. Lisdat, M. Filzinger, N. Huntemann, E. Peik, and T. E. Mehlstäubler, An $^{115}\text{In}^+ - ^{172}\text{Yb}^+$ coulomb crystal clock with 2.5×10^{-18} systematic uncertainty, arXiv:2402.16807 (2024).
- [22] E. Peik, B. Lipphardt, H. Schnatz, T. Schneider, C. Tamm, and S. G. Karshenboim, Limit on the present temporal variation of the fine structure constant, *Phys. Rev. Lett.* **93**, 170801 (2004).
- [23] L. S. Dreissen, C.-H. Yeh, H. A. Füst, K. C. Gremse-mann, and T. E. Mehlstäubler, Improved bounds on Lorentz violation from composite pulse Ramsey spectroscopy in a trapped ion, *Nature Communications* **13**, 7314 (2022).
- [24] J. Hur, D. P. L. Aude Craik, I. Counts, E. Knyazev, L. Caldwell, C. Leung, S. Pandey, J. C. Berengut, A. Geddes, W. Nazarewicz, P.-G. Reinhard, A. Kawasaki, H. Jeon, W. Jhe, and V. Vuletić, Evidence of two-source king plot nonlinearity in spectroscopic search for new boson, *Phys. Rev. Lett.* **128**, 163201 (2022).
- [25] M. Door, C.-H. Yeh, M. Heinz, F. Kirk, C. Lyu, T. Miyagi, J. C. Berengut, J. Bieroń, K. Blaum, L. S. Dreissen, S. Eliseev, P. Filianin, M. Filzinger, E. Fuchs, H. A. Füst, G. Gaigalas, Z. Harman, J. Herkenhoff, N. Huntemann, C. H. Keitel, K. Kromer, D. Lange, A. Rischka, C. Schweiger, A. Schwenk, N. Shimizu, and T. E. Mehlstäubler, Search for new bosons with ytterbium isotope shifts (2024), arXiv:2403.07792 [physics.atom-ph].
- [26] P. Taylor, M. Roberts, S. V. Gateva-Kostova, R. B. M. Clarke, G. P. Barwood, W. R. C. Rowley, and P. Gill, Investigation of the $^2S_{1/2} - ^2D_{5/2}$ clock transition in a single ytterbium ion, *Phys. Rev. A* **56**, 2699 (1997).
- [27] P. J. Blythe, S. A. Webster, H. S. Margolis, S. N. Lea, G. Huang, S.-K. Choi, W. R. C. Rowley, P. Gill, and R. S. Windeler, Subkilohertz absolute-frequency measurement of the 467-nm electric octupole transition in $^{171}\text{Yb}^+$, *Phys. Rev. A* **67**, 020501 (2003).
- [28] T. Schneider, E. Peik, and C. Tamm, Sub-hertz optical frequency comparisons between two trapped $^{171}\text{Yb}^+$ ions, *Phys. Rev. Lett.* **94**, 230801 (2005).
- [29] H. A. Füst, C.-H. Yeh, D. Kalincev, A. P. Kulosa, L. S. Dreissen, R. Lange, E. Benkler, N. Huntemann, E. Peik, and T. E. Mehlstäubler, Coherent excitation of the highly forbidden electric octupole transition in $^{172}\text{Yb}^+$, *Phys. Rev. Lett.* **125**, 163001 (2020).
- [30] A. S. Bell, P. Gill, H. A. Klein, A. P. Levick, C. Tamm, and D. Schnier, Laser cooling of trapped ytterbium ions using a four-level optical-excitation scheme, *Phys. Rev. A* **44**, R20 (1991).
- [31] P. Taylor, M. Roberts, G. M. Macfarlane, G. P. Barwood, W. R. C. Rowley, and P. Gill, Measurement of the infrared $^2F_{7/2} - ^2D_{5/2}$ transition in a single $^{171}\text{Yb}^+$ ion, *Phys. Rev. A* **60**, 2829 (1999).
- [32] S. Olmschenk, D. Hayes, D. N. Matsukevich, P. Maunz, D. L. Moehring, K. C. Younge, and C. Monroe, Measurement of the lifetime of the $6p\ ^2P_{1/2}^o$ level of Yb^+ , *Phys. Rev. A* **80**, 022502 (2009).
- [33] H. M. Meyer, M. Steiner, L. Ratschbacher, C. Zipkes, and M. Köhl, Laser spectroscopy and cooling of Yb^+ ions on a deep-uv transition, *Phys. Rev. A* **85**, 012502 (2012).
- [34] T. Feldker, H. Füst, N. V. Ewald, J. Joger, and R. Gerritsma, Spectroscopy of the $^2S_{1/2} \rightarrow ^2P_{3/2}$ transition in Yb II : Isotope shifts, hyperfine splitting, and branching ratios, *Phys. Rev. A* **97**, 032511 (2018).
- [35] T. Tan, C. Edmunds, A. Milne, M. Biercuk, and C. Hempel, Precision characterization of the $^2D_{5/2}$ state and the quadratic Zeeman coefficient in $^{171}\text{Yb}^+$, *Physical Review A* **104**, L010802 (2021).
- [36] P. T. H. Fisk, M. J. Sellars, M. A. Lawn, and C. Coles, Accurate measurement of the 12.6 GHz clock transition in trapped $^{171}\text{Yb}^+$ ions, *IEEE Trans. Ultrason. Ferroelectr. Freq. Control* **44**, 344 (1997).
- [37] M. Mazzanti, *Trapped ions in optical tweezers and their applications to quantum computing*, Ph.D. thesis, Universiteit van Amsterdam (2023).
- [38] N. Yu and L. Maleki, Lifetime measurements of the $4f^{14}5d$ metastable states in single ytterbium ions, *PRA* **61**, 022507 (2000).
- [39] M. Schacht, J. Danielson, S. Rahaman, J. Torgerson, J. Zhang, and M. M. Schauer, $^{171}\text{Yb}^+ 5D_{3/2}$ hyperfine state detection and $F = 2$ lifetime, *Journal of Physics B: Atomic, Molecular and Optical Physics* **48**, 065003 (2015).
- [40] H. Hirzler, T. Feldker, H. Füst, N. V. Ewald, E. Trimby, R. S. Lous, J. D. Arias Espinoza, M. Mazzanti, J. Joger, and R. Gerritsma, Experimental setup for studying an ultracold mixture of trapped $\text{Yb}^+ - ^6\text{Li}$, *Phys. Rev. A* **102**, 033109 (2020).
- [41] N. V. Ewald, *Quest for an Ultracold Hybrid Atom-Ion Experiment*, Master's thesis, Johannes Gutenberg Universität Mainz (2015).
- [42] A. Urech, I. H. A. Knottnerus, R. J. C. Spreeuw, and F. Schreck, Narrow-line imaging of single strontium atoms in shallow optical tweezers, *Phys. Rev. Res.* **4**, 023245 (2022).
- [43] I. Courtillot, A. Quessada-Vial, A. Bruschi, D. Kolker, G. D. Rovera, and P. Lemonde, Accurate spectroscopy of Sr atoms, *The European Physical Journal D - Atomic, Molecular, Optical and Plasma Physics* **33**, 161 (2005).
- [44] High Finesse GmbH, (2024), private communication.
- [45] C. L. Edmunds, T. R. Tan, A. R. Milne, A. Singh, M. J. Biercuk, and C. Hempel, Scalable hyperfine qubit state detection via electron shelving in the $^2D_{5/2}$ and $^2F_{7/2}$ manifolds in $^{171}\text{Yb}^+$, *Phys. Rev. A* **104**, 012606 (2021).
- [46] C. Roman, *Expanding the $^{171}\text{Yb}^+$ toolbox: the $^2F_{7/2}$ state as resource for quantum information science*, Ph.D. thesis, UNIVERSITY OF CALIFORNIA (2021).
- [47] J. Kwon, W. J. Setzer, M. Gehl, N. Karl, J. Van Der Wall, R. Law, M. G. Blain, D. Stick, and H. J. McGuinness, Multi-site integrated optical addressing of trapped ions, *Nature Communications* **15**, 3709 (2024).